AIP Applied Physics Letters

Grating-coupled mid-infrared light emission from tensilely strained germanium nanomembranes

Cicek Boztug, José R. Sánchez-Pérez, Jian Yin, Max G. Lagally, and Roberto Paiella

Citation: Appl. Phys. Lett. **103**, 201114 (2013); doi: 10.1063/1.4830377
View online: http://dx.doi.org/10.1063/1.4830377
View Table of Contents: http://apl.aip.org/resource/1/APPLAB/v103/i20
Published by the AIP Publishing LLC.

Grating-coupled mid-infrared light emission from tensilely strained germanium nanomembranes

Cicek Boztug,[1] José R. Sánchez-Pérez,[2] Jian Yin,[1] Max G. Lagally,[2,a)] and Roberto Paiella[1,b)]
[1]Department of Electrical and Computer Engineering and Photonics Center, Boston University, 8 Saint Mary's Street, Boston, Massachusetts 02215, USA
[2]Department of Materials Science and Engineering, University of Wisconsin–Madison, 1509 University Ave., Madison, Wisconsin 53706, USA

(Received 30 August 2013; accepted 31 October 2013; published online 14 November 2013)

Mechanically stressed nanomembranes are used to demonstrate mid-infrared interband light emission from Ge within the 2.1–2.5 μm atmospheric transmission window. Large biaxial tensile strain is introduced in these samples to convert Ge into a (near-) direct-bandgap semiconductor and to red-shift its luminescence. A diffractive array of Ge pillars is used to outcouple the long-wavelength interband radiation, which is otherwise primarily emitted in the sample plane. An order-of-magnitude strain-induced enhancement in radiative efficiency is also reported, together with the observation of luminescence signatures associated with photonic-crystal cavity modes. These results are promising for the development of silicon-compatible lasers for mid-infrared optoelectronics applications. © *2013 AIP Publishing LLC*. [http://dx.doi.org/10.1063/1.4830377]

Germanium has been widely investigated in recent years as a promising candidate for the development of group-IV semiconductor lasers that can be monolithically integrated with complementary metal-oxide-semiconductor (CMOS) microelectronics. In fact, despite its indirect-bandgap nature, substantial light emission can be obtained from Ge in the presence of biaxial tensile strain, which has the effect of decreasing the difference between the direct- and indirect-bandgap energies.[1–7] As a result, in tensilely strained Ge under electrical or optical pumping, a sizeable fraction of the injected electrons can thermalize near the direct conduction-band minimum, where efficient recombination via interband light emission takes place. In a recent report,[8] a small amount of tensile strain (0.25%, introduced in plastically relaxed Ge on Si via an anneal process) has been combined with highly degenerate *n*-type doping to demonstrate a near-infrared Ge diode laser operating at a wavelength near 1550 nm. At higher strain levels (above 1.4% biaxial according to the calculations of Ref. 9), population inversion and optical gain can also be obtained without any doping, which is desirable for the purpose of minimizing the deleterious effects of free-carrier absorption and nonradiative Auger recombination. If the biaxial strain is further increased above 1.9%, Ge is even transformed into a direct-bandgap semiconductor, like the active materials of traditional III–V diode lasers.

Biaxial tensile strain in Ge also causes the direct-bandgap energy, and therefore the interband emission wavelength, to red-shift into the mid-infrared spectral region. This behavior follows from the strong decrease of the conduction band minimum at the direct (Γ) point of reciprocal space with increasing tensile strain. At the same time, the valence band maxima increase and their degeneracy is lifted, with the light-hole (LH) band pushed up in energy relative to the heavy-hole (HH) band. At the aforementioned strain levels required for optical gain, the Ge bandgap energy is red-shifted into the atmospheric transmission window between 2.1 and 2.5 μm.[9] This spectral region is technologically significant for applications in biological and chemical sensing (e.g., trace-gas detection, environmental monitoring, medical diagnostics, and industrial process control), as well as spectroscopy and secure free-space optical communications. The development of CMOS compatible diode lasers based on tensilely strained Ge could therefore enable extending the large-scale on-chip integration of electronic and photonic functionalities to address these important application areas.[10]

Motivated by these considerations, a number of groups have recently investigated different methods to introduce large tensile strain in crystalline Ge. These methods include heteroepitaxial growth on suitable substrates such as InGaAs[11,12] and SiGeSn,[3,13] the use of stressor layers,[14–17] and the application of external mechanical stress.[9,18–20] A common feature of these approaches is the use of Ge samples with nanoscale dimensions, because the smaller the sample volume the larger the maximum strain that can be introduced before the onset of plastic deformation and cracking. For externally applied biaxial stress, particularly large strain is obtained with Ge nanomembranes (NMs), i.e., single-crystal sheets with a thickness of only a few tens of nanometers that are either completely released from, or partially suspended over, their native rigid substrate.[21] In Ref. 20, mechanically stressed Ge NMs have been used to demonstrate straining beyond the accepted threshold for direct-bandgap behavior, together with substantial strain-enhanced photoluminescence (PL) and evidence of population inversion under optical pumping.

Despite this recent progress, appreciable mid-infrared light emission from biaxially tensilely strained Ge has not yet been demonstrated, with all previously reported luminescence spectra peaked at wavelengths below 2 μm. This limitation is the result of unfavorable polarization selection

a)Electronic mail: lagally@engr.wisc.edu
b)Electronic mail: rpaiella@bu.edu

rules. Under biaxial tensile strain, light emission near the direct-bandgap edge involves transitions between the conduction band and the LH valence band, due to the aforementioned strain-induced splitting of the valence bands. The resulting luminescence is predominantly transverse-magnetic (TM), i.e., linearly polarized in the direction perpendicular to the faces of the strained layer, as a result of the symmetry properties of the LH Bloch functions.[9] This luminescence necessarily propagates on the plane of the emissive film and therefore cannot be collected in standard surface-emission measurements. As a result, the experimental spectra are dominated by conduction-to-heavy-hole (cΓ-HH) transitions that produce transverse-electric (TE) light at shorter wavelengths, despite the smaller hole population of the HH band caused by its lower energy. In Ref. 20, evidence of conduction-to-light-hole (cΓ-LH) emission under high tensile strain was observed, but only in the form of a relatively weak long-wavelength shoulder in the predominantly cΓ-HH emission spectra. Furthermore, the measured increase in luminescence efficiency brought about by the applied stress was limited to values of about 4×. This observation can be ascribed to the same unfavorable polarization selection rules, as most of the strain-enhanced emission is TM polarized and therefore could not be detected.

To address these limitations, in the present work we develop Ge NMs patterned with a two-dimensional grating that allows for efficient extraction of the in-plane-emitted light via first-order diffraction. The key challenge in the design of such structures is related to the highly sub-wavelength nanoscale thickness of the Ge emissive layer, which is necessary in order to enable the introduction of sufficiently large biaxial strain levels without plastic deformation. At the same time, an optically thick overall structure is required to provide efficient vertical outcoupling of the emitted light, via diffractive scattering of well-confined in-plane guided modes. To meet these conflicting requirements, we employ a periodic array of amorphous Ge (a-Ge) pillars fabricated on an ultrathin NM, effectively forming a two-dimensional photonic-crystal slab. These arrays can, in principle, be made arbitrarily thick, with a large average refractive index and strong index contrast between the pillars and the surrounding medium. At the same time, by virtue of their disconnected nature, their presence only negligibly compromises the mechanical flexibility of the underlying NM. In the resulting geometry, the in-plane-emitted TM-polarized light is mostly guided in the high-index NM/array layer, where it propagates with an effective index n_{eff}. By first-order diffraction, this guided mode can be scattered into radiation propagating along the sample surface normal if its free-space wavelength λ is close to the Bragg condition $\lambda = n_{eff}\,\Lambda$, where Λ is the array period (e.g., see Ref. 22). Furthermore, light at neighboring wavelengths can be diffracted out of the sample along oblique directions. As a result, the grating allows measuring in-plane-emitted light over a relatively broad wavelength range, ultimately determined by the numerical aperture of the lens used to collect the sample luminescence.

The Ge NMs used in this work are fabricated from (001) Ge-on-insulator (GOI) substrates, whose Ge template layer is first thinned down to the desired thickness of about 30 nm (thin enough to allow for the introduction of the required strain levels without extended-defect formation[20]). Next, the NM boundaries are patterned through the template layer by photolithography. The underlying buried oxide is then removed with a wet etch in a 49% hydrofluoric-acid solution, with the photoresist temporarily left on the sample to act as a weak stressor layer that facilitates the NM release. After the wet etch, the sample is quickly submerged in deionized water before the NMs can attach to the Si host wafer. Finally, a wire loop is used to harvest the NMs from the water surface and transfer them to a 125 μm-thick flexible polyimide (PI) film, where they initially settle via hydrogen and van der Waals bonding and are then more firmly bonded by annealing.

Array fabrication employs electron-beam lithography to pattern a square-periodic array of cylindrical holes in a poly(methyl-methacrylate) (PMMA) resist previously spun on the NM. Amorphous Ge is then deposited on the patterned PMMA by electron-beam evaporation, followed by lift-off. The end result is a regular array of Ge pillars featuring sloped sidewalls, as illustrated in the scanning electron microscopy (SEM) image of Fig. 1(a). Finally, a relatively thick (about 3 μm) PI coating is spun over the array in order to produce a symmetric dielectric environment around the high-index NM/array layer, which improves the vertical optical confinement of the emitted light and its overlap with the grating. A schematic cross-sectional view of the resulting device structure is shown in the inset of Fig. 1(a).

To introduce strain, the PI film with the attached NM is introduced into an otherwise rigid cavity, which is then filled with high-pressure gas, as shown schematically in Fig. 1(b). In this configuration, effectively a bending mode, maximum biaxial tensile strain is created at the top surface of the stretched film. Relative to our earlier measurements[20] in which the Ge NM was the top surface, here the presence of the array and of the PI coating must, in principle, decrease the amount of strain introduced in the NM for any given

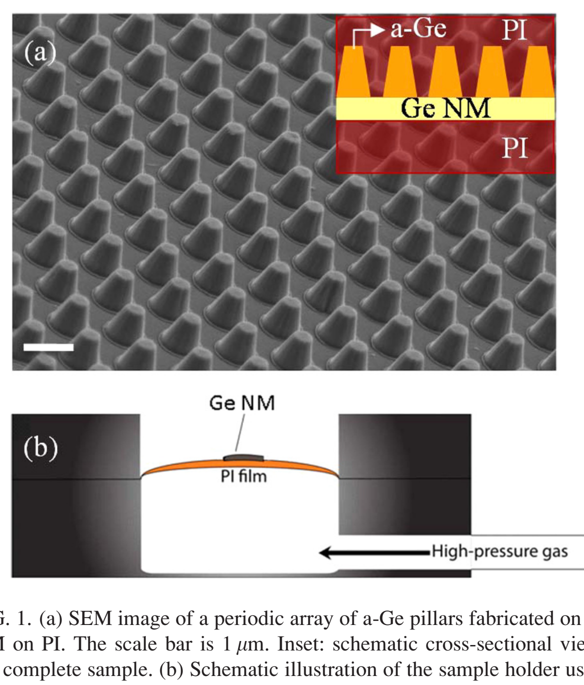

FIG. 1. (a) SEM image of a periodic array of a-Ge pillars fabricated on a Ge NM on PI. The scale bar is 1 μm. Inset: schematic cross-sectional view of the complete sample. (b) Schematic illustration of the sample holder used to introduce biaxial tensile strain in the NM.

pressure. Calculations taking into account thicknesses and bulk moduli indicate, however, that in the present geometry this strain reduction is negligible (of the order of 4% of the maximum strain at the film top surface).

For PL measurements, the NM is excited with a tunable optical parametric oscillator, which produces a train of pulses with 5 ns duration, 20 Hz repetition rate, and 945 nm wavelength. The pump light is focused onto the gratings with a spot size of about 1 mm. The emitted light is collected from the NM top surface with an *f*/1 lens, dispersed through a monochromator, and finally measured using a room-temperature extended-range InGaAs photodetector with 1.2–2.6 μm spectral response and 45 MHz bandwidth. To increase the measurement sensitivity, gated detection is performed using a box-car integrator. The measured PL spectra are finally normalized to the spectral response of the setup, which is determined by the reflectivity of the monochromator grating and the responsivity of the photodiode.

In Fig. 2, we show a selection of normalized room-temperature PL spectra measured with a Ge NM/array sample for different values of the applied gas pressure and of the incident average pump power (indicated in the insets). In this sample, the pillar base diameter and the array period Λ are 700 nm and 1280 nm, respectively, as estimated from the SEM images; the nominal pillar height is 300 nm. The fundamental TM mode of this geometry has an effective index n_{eff} of about 1.75, as computed via finite-element simulations by modeling the entire structure as a planar dielectric waveguide. Specifically, in these calculations the refractive indexes of Ge and PI were taken to be 4.1 and 1.7, respectively, and the grating layer was treated as a uniform medium described by its average index. The corresponding Bragg wavelength $n_{eff}\Lambda$ is therefore in the neighborhood of 2.3 μm, where strong cΓ-LH emission under high tensile strain is expected. Furthermore, simple considerations based on diffraction theory[22] indicate that the *f*/1 lens used in our measurements can collect in-plane-emitted light, scattered by the array along different directions, over the broad wavelength range of about 1.7–2.8 μm (much broader than the expected linewidth of the cΓ-LH emission peak).

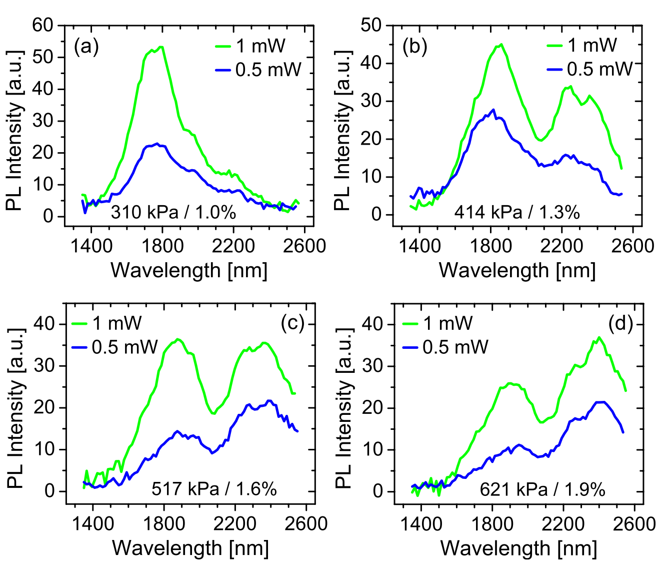

FIG. 2. Normalized PL spectra measured with a Ge NM/array sample for different values of the applied stress and of the average pump power. The estimated values of biaxial tensile strain in the NM, taken from prior Raman data that allow pressure to strain conversion[20] are also listed in each graph.

The ability of this array to outcouple such in-plane-emitted long-wavelength luminescence is well substantiated by the data of Fig. 2. At sufficiently high strain [Figs. 2(b)–2(d)], two emission peaks are clearly resolved, associated with cΓ-HH and cΓ-LH transitions in order of increasing wavelength. As the applied stress is increased, both peaks red-shift while their separation increases and the cΓ-LH feature grows progressively stronger. Eventually, the overall luminescence spectrum becomes dominated by the latter feature, consistent with the higher hole population of the LH band compared to the HH band. This behavior is especially pronounced at the lower pump power used in these measurements (0.5 mW average), where the density of photoexcited holes that can thermalize in the HH band is particularly small. By comparison, in our earlier work[9,20] (where no diffractive arrays were employed) single-peak emission spectra were consistently measured peaked at the shorter cΓ-HH transition wavelength, owing to the predominantly in-plane-propagating nature of the cΓ-LH emission. At the highest applied stress of Fig. 2 [panel (d)], a peak emission wavelength as long as 2.4 μm is obtained. These results directly demonstrate the predicted ability of tensilely strained Ge to provide interband light emission in the technologically important 2.1–2.5 μm mid-infrared atmospheric transmission window.

Also indicated in the insets of Figs. 2(a)–2(d) are the estimated biaxial tensile strain levels correspondingly introduced in the NM. These values were obtained as a function of gas pressure from Raman spectroscopy measurements made earlier on Ge NMs of similar thickness ($\sim$40 nm) mounted on the same sample holder of Fig. 1(b).[20] Based on these values, the variation of the peak emission energies of Fig. 2 with strain is consistent with predictions based on deformation potential theory.[9,20] The highest biaxial strain shown in this figure, 1.9%, suggests that in these measurements the Ge active material was strained close to (if not beyond) the threshold for direct-bandgap behavior. Analysis of the PL spectra of Fig. 2(d) confirms this conclusion. In particular, the cΓ-HH bandgap energy can be accurately determined from the spectral position of the low-pump-power short-wavelength emission peak, as the low density of photoexcited HHs in this measurement ensures minimal band filling effects (i.e., minimal deviation of the emission wavelength from the bandgap energy). The estimated value of 640 meV is lower than the calculated cΓ-HH bandgap energy at the transition point to direct-bandgap Ge (650 meV based on deformation potential theory[9,20]), suggesting that this transition point has in fact been crossed in Fig. 2(d).

Additional information about the properties of the NM/array samples under study can be inferred from their PL spectra measured with higher incident pump power. In Fig. 3(a), we show examples of such spectra, measured with the same sample of Fig. 2 at different strain levels with an average pump power of 3.5 mW. Under such relatively high excitation conditions, the HH band is also appreciably populated with photoexcited holes, at least in the immediate vicinity of the Γ point where most of the electrons within the

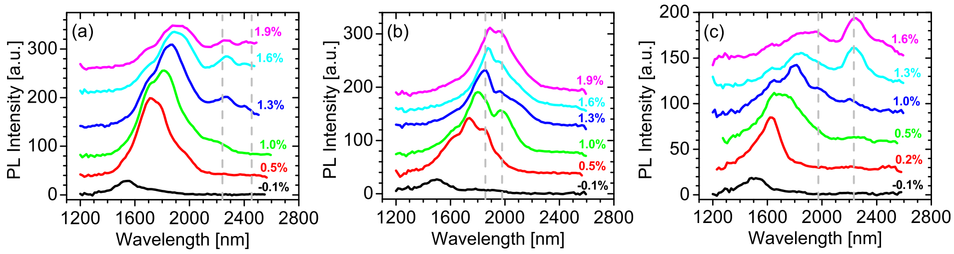

FIG. 3. Strain-resolved normalized PL spectra measured with different Ge NM/array samples under relatively high pumping conditions (3.5 mW average incident pump power). (a) Spectra measured on the sample of Fig. 2. (b) Spectra measured on a sample featuring a smaller array period. (c) Spectra measured on a sample featuring taller pillars and larger array fill factor. In each panel, the vertical dashed lines indicate the calculated wavelengths of the Γ-point TM modes of the array photonic-crystal slab in the spectral vicinity of the cΓ-LH emission.

direct conduction-band minimum reside. As a result, the emission becomes dominated by the cΓ-HH transitions by virtue of their more favorable polarization properties. At the same time, the PL spectrum of the unstrained NM can now be clearly resolved (bottom trace in the figure), which allows estimating the increase in luminescence efficiency brought about by the applied stress. To that purpose, we compare the number of emitted photons (proportional to the normalized PL intensity spectrum divided by photon energy and integrated over all wavelengths) with and without stress. With this procedure, we find a large PL efficiency enhancement of about 11× at a strain level of 1.3%. This enhancement value should be interpreted as a lower bound, as the corresponding PL spectrum extends past the 2.6 μm cutoff of our detection system. For the same reason, slightly smaller values are computed with the higher-strain spectra (which should show even larger efficiencies), since these spectra are red-shifted even farther. By comparison, in our prior work of Ref. 20, a maximum enhancement of only about 4× was measured under similar conditions, limited by the inefficient collection of the in-plane-emitted cΓ-LH luminescence. The results presented in Fig. 3(a), therefore, further substantiate the ability of tensile strain to enhance the radiative properties of Ge NMs.

In addition, two relatively narrow features can also be seen superimposed to the cΓ-LH contribution in the high-strain spectra of Fig. 3(a), centered at a constant (i.e., strain independent) wavelength of 2.27 μm and 2.41 μm, respectively. These features, which are also visible in Fig. 2, are attributed to cavity resonances of the photonic crystal slab formed by the pillar array. In a simple picture, light emitted at these wavelengths can be reflected back and forth in the plane of the NM via second-order diffraction by the array, leading to enhanced output light. For a more quantitative interpretation, we have investigated the photonic band structure of the sample under study via finite-difference time domain (FDTD) simulations, using a two-dimensional model based on the effective-index approximation. The geometrical parameters and index values mentioned previously were employed in these calculations, except for a smaller value of the pillar diameter (590 nm, consistent with the sloped sidewalls of these pillars, and selected so as to maximize agreement with the data). The vertical dashed lines in Fig. 3(a) indicate the calculated wavelengths of the Γ-point TM modes in the spectral region of the cΓ-LH emission. A fair agreement with the measured resonances is obtained, with the observed discrepancies likely due to the implicit assumptions of the model.

Additional evidence of the observation of cavity modes is given in Fig. 3(b), where we plot the strain-resolved PL spectra measured with a different sample having smaller array period (1085 nm) and smaller column diameter (510 nm at the base of the pillars). Two relatively narrow strain-independent features are again observed, but at lower wavelengths (1.87 μm and 1.97 μm), consistent with the reduced array periodicity of this sample and in reasonably good agreement with the FDTD simulation results (again indicated by the dashed lines, obtained by assuming an average pillar diameter of 360 nm). We note that the long-wavelength cΓ-LH luminescence here is not efficiently collected, also because of the smaller period Λ and proportionally smaller Bragg wavelength $n_{eff}\Lambda \approx 1.9\,\mu$m (away from the high-strain cΓ-LH emission band). Finally, in Fig. 3(c), we show similar data obtained with another sample featuring taller (500 nm) pillars with larger (780 nm) base diameter and intermediate (1145 nm) period. By virtue of the larger thickness and higher fill factor (i.e., higher average refractive index) of the array, this sample supports more tightly confined TM modes that can be more effectively diffracted by the pillars. Correspondingly, the high-strain emission spectra are now fully dominated by a cavity resonance at 2.24 μm near the peak of the cΓ-LH luminescence. Altogether, these results indicate that the NM/array geometry under study provides a suitable platform for the development of optical cavities compatible with the flexibility requirements of mechanically stressed active layers.

This work was primarily supported by the National Science Foundation under Grant #DMR-0907296. The NM fabrication activities (J.R.S.-P. and M.G.L.) and growth facilities maintenance were supported by the Department of Energy (Grant #DE-FG02-03ER46028).

[1] R. A. Soref and L. Friedman, Superlattices Microstruct. **14**, 189 (1993).
[2] M. V. Fischetti and S. E. Laux, J. Appl. Phys. **80**, 2234 (1996).
[3] J. Menéndez and J. Kouvetakis, Appl. Phys. Lett. **85**, 1175 (2004).
[4] J. Liu, X. Sun, D. Pan, X. Wang, L. C. Kimerling, T. L. Koch, and J. Michel, Opt. Express **15**, 11272 (2007).
[5] P. H. Lim, S. Park, Y. Ishikawa, and K. Wada, Opt. Express **17**, 16358 (2009).
[6] M. El Kurdi, G. Fishman, S. Sauvage, and P. Boucaud, J. Appl. Phys. **107**, 013710 (2010).
[7] G. Pizzi, M. Virgilio, and G. Grosso, Nanotechnology **21**, 055202 (2010).
[8] R. E. Camacho-Aguilera, Y. Cai, N. Patel, J. T. Bessette, M. Romagnoli, L. C. Kimerling, and J. Michel, Opt. Express **20**, 11316 (2012).
[9] C. Boztug, J. R. Sánchez-Pérez, F. F. Sudradjat, R. B. Jacobson, D. M. Paskiewicz, M. G. Lagally, and R. Paiella, Small **9**, 622 (2013).

[10]R. Soref, Nature Photon. **4**, 495 (2010).
[11]Y. Huo, H. Lin, R. Chen, M. Makarova, Y. Rong, M. Li, T. I. Kamins, J. Vuckovic, and J. S. Harris, Appl. Phys. Lett. **98**, 011111 (2011).
[12]R. Jakomin, M. de Kersauson, M. El Kurdi, L. Largeau, O. Mauguin, G. Beaudoin, S. Sauvage, R. Ossikovski, G. Ndong, M. Chaigneau, I. Sagnes, and P. Boucaud, Appl. Phys. Lett. **98**, 091901 (2011).
[13]Y. Y. Fang, J. Tolle, R. Roucka, A. V. G. Chizmeshya, J. Kouvetakis, V. R. D'Costa, and J. Menéndez, Appl. Phys. Lett. **90**, 061915 (2007).
[14]M. de Kersauson, M. El Kurdi, S. David, X. Checoury, G. Fishman, S. Sauvage, R. Jakomin, G. Beaudoin, I. Sagnes, and P. Boucaud, Opt. Express **19**, 17925 (2011).
[15]D. Nam, D. Sukhdeo, A. Roy, K. Balram, S. Cheng, K. Huang, Z. Yuan, M. Brongersma, Y. Nishi, D. Miller, and K. Saraswat, Opt. Express **19**, 25866 (2011).
[16]J. R. Jain, A. Hryciw, T. M. Baer, D. A. B. Miller, M. L. Brongersma, and R. T. Howe, Nature Photon. **6**, 398 (2012).
[17]M. J. Süess, R. Geiger, R. A. Minamisawa, G. Schiefler, J. Frigerio, D. Chrastina, G. Isella, R. Spolenak, J. Faist, and H. Sigg, Nature Photon. **7**, 466 (2013).
[18]M. El Kurdi, H. Bertin, E. Martincic, M. de Kersauson, G. Fishman, S. Sauvage, A. Bosseboeuf, and P. Boucaud, Appl. Phys. Lett. **96**, 041909 (2010).
[19]T. H. Cheng, K. L. Peng, C. Y. Ko, C. Y. Chen, H. S. Lan, Y. R. Wu, C. W. Liu, and H. H. Tseng, Appl. Phys. Lett. **96**, 211108 (2010).
[20]J. R. Sánchez-Pérez, C. Boztug, F. Chen, F. F. Sudradjat, D. M. Paskiewicz, R. Jacobson, M. G. Lagally, and R. Paiella, Proc. Natl. Acad. Sci. U.S.A. **108**, 18893 (2011).
[21]J. A. Rogers, M. G. Lagally, and R. G. Nuzzo, Nature **477**, 45 (2011).
[22]S. L. Chuang, *Physics of Photonic Devices* (Wiley, Hoboken, NJ, 2009), pp. 297–300.